Solid State Phenomena
ISSN: 1662-9779, Vol. 388, pp 153-162
doi:10.4028/p-IUrc7E

Submitted: 2026-01-19
Revised: 2026-02-16
Accepted: 2026-02-20
Online: 2026-04-15

Hole Expansion Performance Assessment of Quenched and Partitioning Steel Through a Fully Anisotropic Fracture Modeling

Toros Arda Aksen[1,2,a], Zinan Li[1,b] and Junhe Lian[1,3,c*]

[1]Department of Energy and Mechanical Engineering, Aalto University, 02150, Espoo, Finland

[2]Mechanical Engineering Department, Sakarya University, 54050, Sakarya, Türkiye

[3]Institute of Metal Forming, RWTH Aachen University, 52072, Aachen, Germany

[a]ardaaksen@sakarya.edu.tr, [b]zinan.li@aalto.fi, [c*]junhe.lian@ibf.rwth-aachen.de

[*]corresponding author

Keywords: QP steel, local formability, edge crack, fully anisotropic fracture model.

Abstract. Edge cracking is an essential local formability phenomenon encountered in specific forming operations, such as stretch flanging, which is broadly employed in the automotive industry. However, the prediction of the edge cracks is challenging, and the hole expansion test is widely carried out to detect the edge cracking performance. This research analyzed quenched and partitioned steel (QP), one of the third-generation advanced high-strength steels widely adopted in the automotive industry to replace conventional high-strength steels due to its superior global formability features. However, its local formability has been a bottleneck due to its microstructure nature and shows strong anisotropy dependency. Therefore, a modeling framework is needed that consistently incorporates anisotropy in both plasticity and fracture. In this study, the hole expansion performance of QP1000 steel was evaluated through a fully anisotropic fracture model based on the Yld2004-18p anisotropic yield criterion and the DF2016 ductile fracture model. To this end, the standard uniaxial tensile tests in seven material orientations, the bulge test, and the tensile tests of different fracture samples were conducted. These samples were picked out to characterize the broad spectrum of loading conditions and cut in rolling, diagonal, and transverse directions to establish the fully anisotropic fracture model. It was seen that the edge cracking metrics, which are the hole expansion ratio and the fracture initiation zone, were accurately captured by the developed model.

Introduction

The transportation sector causes a considerable amount of harmful gas emissions, and road vehicles have a major role in these emissions [1]. Therefore, the international regulations and competition between the automotive companies necessitate the automotive industry to have a primary aim to decrease harmful gas emissions. In this framework, the automotive companies tended to develop new technologies in lightweight materials. Advanced high-strength steels (AHSS) are one of these materials, and Quenched and Partitioning steels (QP) are the salient steels to replace the conventional high-strength steels in the automotive industry [2, 3]. The QP steel ensured the high strength and formability relative to the other AHSSs; however, edge cracking is a vital topic in these steels. Certain AHSSs demonstrate low edge cracking performance [4, 5], and the studies on the edge cracking phenomenon in QP steels are limited.

Edge cracking is a local formability feature where deformation is localized in specific regions, which is difficult to detect. The hole expansion test is conducted to evaluate the edge cracking performance, and numerous studies in the literature have examined the hole expansion performance of AHSSs. Chung et al. [4] investigated the hole expansion performance of TRIP590 and TWIP940 steels in terms of hole expansion ratio (HER). They pointed out that the TWIP steel exhibited poor hole expansion performance. Barnval et al. [6] carried out a similar study on first-generation AHSSs, namely DP and TRIP steels. Firat et al. [7] conducted a study to assess the local formability features of DP steels. Recently. Li et al.[8] investigated the edge fracture of DP1000 steel and discovered that anisotropy-introduced localization has been the trigger of the final fracture. In all

these studies, the significance of an advanced anisotropic yield criterion in local formability was emphasized.

Contrary to the first and second generation AHSSs, the studies related to the local formability of third generation steels, especially QP steel, are limited. Madrid et al. [9] assessed the effect of edge conditions and the punch geometry on the edge cracking performance of QP steels. Li et al [10] conducted a study related to the fracture performance of QP1000 steel. They used the Hill48 criterion with crucial modifications and performed the fully anisotropic fracture modeling. There are also different studies related to the fracture of QP steels [11-15]. However, studies relevant to the edge cracking predictions are limited, and numerical studies mostly include basic anisotropic yield criteria or isotropic yield criteria [14, 15]. A recent study by Aksen et al. [16] applied several anisotropic yield criteria, including different Hill formulations, and the Yld2004-18p model on QP1000 steel, and they revealed that only Yld2004-18p can predict the location of the edge fracture accurately. However, due to the nature of the isotropic formulation of the fracture criterion, the model still fails to predict the HER value correctly. Therefore, a fully anisotropic fracture model in conjunction with an advanced anisotropic plasticity model is essential to evaluate the edge cracking properties of QP1000 steel.

This study evaluates the performance of fully anisotropic fracture modeling in predicting edge cracking of QP1000 steel in HET. In this framework, a material model including the Yld2004-18p anisotropic yield criterion, coupled with the DF2016 ductile fracture model, was adopted. Standard uniaxial tensile tests (SDB) were conducted in seven orientations, covering from the rolling direction (RD) to the transverse direction (TD). To include the biaxial data in the yield criterion calibration, a bulge test was conducted. In addition, fracture samples, including a centered hole sample (CH), radius-shaped notched samples (NDBR), and a shear sample, were employed to characterize the fracture mechanism across a wide spectrum of loading conditions. Furthermore, these fracture samples were cut in three orientations to represent the fully anisotropic fracture model. Afterward, the hole expansion test of QP1000 steel with a conical punch configuration was performed in order to observe the edge cracking metrics, and the finite element (FE) analyses were conducted. The prediction performance of the calibrated model was evaluated in terms of edge cracking metrics in QP1000 steel in the hole expansion test.

Mechanical Testing

The standard uniaxial tensile test samples of QP1000 steel were cut in seven orientations from RD to TD (0°, 15°, 30°, 45°, 60°, 75°, 90°) with a thickness of 1.36 mm [10, 16], and the tests were carried out in compliance with the ISO6892 specifications under quasi-static testing rates using Zwick-Roell screw-driven tensile testing machine with an extensometer of 30 mm gauge length. The result of the RD sample was used to adjust the hardening behavior of QP1000 steel. Fig. 1 shows the engineering stress-strain curves acquired from the SDB samples and the hardening curve based on mixed Swift-Voce type hardening law (The parameters are given in ref. [10]).

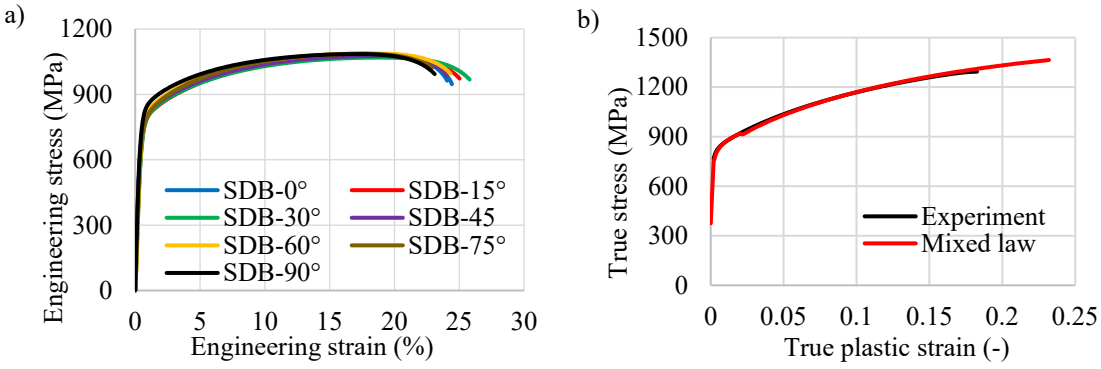

Fig. 1. a) Engineering stress-strain behaviors in different orientations and b) flow curve in RD for QP1000 steel.

The r values and stress ratios were obtained from the SDB sample tests conducted at various strain levels. The r values tend to saturate at the strain level corresponding to ultimate tensile stress; therefore, the strain values at the saturation point were regarded. However, the stress ratios varied throughout the deformation. In this regard, the stress ratios at 0.05 strain level were regarded in order to represent the general behavior of the variation. Table 1 shows the r values and stress ratios considered in this study.

Table 1. Engineering stress-strain behaviors in different orientations for QP1000 steel.

Orientation (deg.)	0°	15°	30°	45°	60°	75°	90°
Stress ratio (σ_θ)	1	1.004	0.995	0.996	1.019	1.021	1.027
r value (r_θ)	0.75	0.65	0.73	0.91	0.71	0.7	0.86

Afterwards, the fracture test samples were conducted in RD, diagonal direction (DD), as well as TD. The dimensions and the testing conditions are explained in [10]. The force-displacement behaviors of fracture samples are given in Fig. 2 for three orientations. These experimental data, including the SDB data, can also be accessed via Zenodo repositories [17].

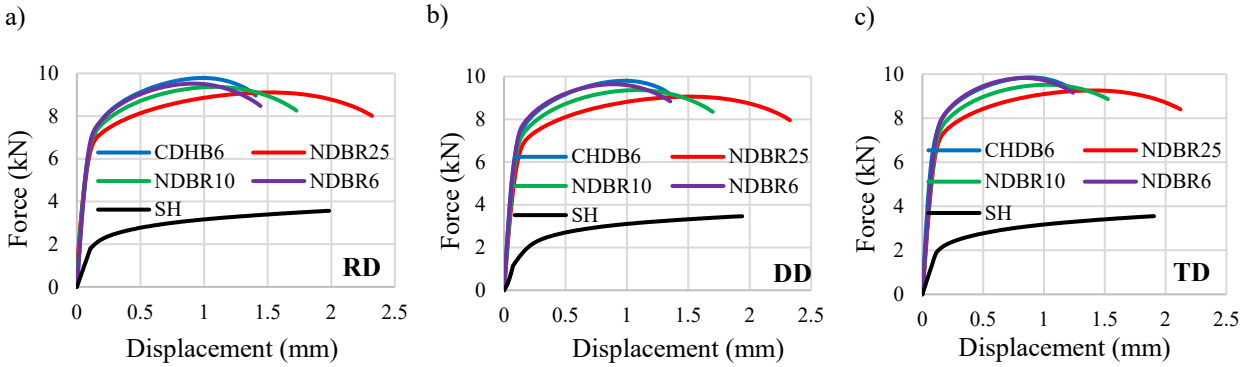

Fig. 2. Force-displacement behaviors of fracture samples in a) RD, b) DD, and c) TD.

The QP1000 steel did not demonstrate a significant difference in force-displacement behaviors along three orientations; however, ductility decreased noticeably in TD orientations, indicating that anisotropic ductility is an essential feature of QP1000 steel. To specify the biaxial r value and stress ratio, a bulge test was conducted with a square sample of 230 mm length. Punch moved at a rate of 3 mm/min while the sample was clamped with a holder force of 600 kN. Comprehensive information can also be found in [8], including the dimensions of the tools. In the final stage, an HET was conducted in accordance with the ISO 16630 specifications. The 10 mm hole was cut by electro discharging machine to ensure a higher hole edge surface quality. Thus, the microcracks due to the punch process were diminished. The hole was expanded through a conical punch with an apex angle of 60°. The blanking force was applied as 235 kN to a circular blank with a radius of 90 mm. In the meantime, the punch moved at a constant rate of 5 mm/min. The sample was tested until a through-thickness crack (TTC) occurred.

Constitutive Modeling

Within the scope of this research, an anisotropic plasticity model was considered. In this perspective, the Yld2004-18p yield criterion was adopted to characterize the material anisotropy. In order to account for the fracture mechanism, the DF2016 ductile fracture model was implemented.

Plasticity Model.

The Yld2004-18 yield criterion encompasses the r value and stress ratio directionalities, in addition to the biaxial data. This criterion is expressed as in Eq. 1 [18].

$$f_{Yld2004-18p} = |S_1' - S_1''|^m + |S_1' - S_2''|^m + |S_1' - S_3''|^m + |S_2' - S_1''|^m + |S_2' - S_2''|^m + |S_2' - S_3''|^m + |S_3' - S_1''|^m + |S_3' - S_2''|^m + |S_3' - S_3''|^m = 4\sigma_{eq}^m \,. \quad (1)$$

Here, S_{1-3}' and S_{1-3}'' denote the principal stresses of the first and second linear transformed-deviatoric stress components. The first and second linear transformations of the deviatoric stress tensors are given in Eq. 2 and Eq. 3.

$$\mathbf{S}' = \mathrm{S_{ij}'} = \mathrm{C_{ij}'T_{ij}\sigma_{ij}} = \begin{bmatrix} 0 & -\alpha_1 & -\alpha_2 & 0 & 0 & 0 \\ -\alpha_3 & 0 & -\alpha_4 & 0 & 0 & 0 \\ -\alpha_5 & -\alpha_6 & 0 & 0 & 0 & 0 \\ 0 & 0 & 0 & \alpha_7 & 0 & 0 \\ 0 & 0 & 0 & 0 & \alpha_8 & 0 \\ 0 & 0 & 0 & 0 & 0 & \alpha_9 \end{bmatrix} \begin{bmatrix} S_{xx} \\ S_{yy} \\ S_{zz} \\ S_{yz} \\ S_{zx} \\ S_{xy} \end{bmatrix}. \quad (2)$$

$$\mathbf{S}'' = S_{ij}'' = C_{ij}'' T_{ij} \sigma_{ij} = \begin{bmatrix} 0 & -\alpha_{10} & -\alpha_{11} & 0 & 0 & 0 \\ -\alpha_{12} & 0 & -\alpha_{13} & 0 & 0 & 0 \\ -\alpha_{14} & -\alpha_{15} & 0 & 0 & 0 & 0 \\ 0 & 0 & 0 & \alpha_{16} & 0 & 0 \\ 0 & 0 & 0 & 0 & \alpha_{17} & 0 \\ 0 & 0 & 0 & 0 & 0 & \alpha_{18} \end{bmatrix} \begin{bmatrix} S_{xx} \\ S_{yy} \\ S_{zz} \\ S_{yz} \\ S_{zx} \\ S_{xy} \end{bmatrix}. \quad (3)$$

In Eqs. 1 and 2, the α_i parameters refer to the anisotropy parameters that need to be optimized based on the yield conditions in different orientations and the balanced-biaxial loading. For the optimization process, the least squares method was employed. The associated flow rule for the relation between plastic potential and plastic strain increment is given in Eq. 4.

$$\dot{\boldsymbol{\varepsilon}}^{\boldsymbol{p}} = d\varepsilon_{ij}^p = d\lambda \frac{\partial f_{Yld2004}}{\partial \sigma_{ij}} \,. \quad (4)$$

Finally, the isotropic hardening rule was considered, which is represented by the mixed hardening law encompassing the Swift-Voce laws given in Eq. 5.

$$\sigma_{Modulated} = \alpha(C(\varepsilon_0 + \varepsilon_{pl})^p) + (1-\alpha)\left(k_0 + Q\left(1 - e^{-b\varepsilon_{pl}}\right)\right). \quad (5)$$

Fully Anisotropic Fracture Model.

Similar to Li et al. [10], a fully anisotropic fracture model was established to reflect the variation in fracture strain with different material orientations, considering the linear transformation of plastic strain components at fracture, which simplifies calibration and implementation. To this end, five different fracture samples were tested in three orientations, namely RD, DD, and TD. For each sample, the plastic strain components at fracture were procured from the FE analyses, and their transformations were regarded. The transformed strain increment tensor ($\dot{\boldsymbol{\varepsilon}}^{\boldsymbol{T}} = [\dot{\varepsilon}_{11}^T, \dot{\varepsilon}_{22}^T, \dot{\varepsilon}_{33}^T, \dot{\varepsilon}_{23}^T, \dot{\varepsilon}_{13}^T, \dot{\varepsilon}_{12}^T]$**)** can be expressed by Eq. 6.

$$\dot{\boldsymbol{\varepsilon}}^{\boldsymbol{T}} = \boldsymbol{L}\, \dot{\boldsymbol{\varepsilon}}^{\boldsymbol{p}} \,. \quad (6)$$

Here, **L** is the modified linear transformation tensor given in Eq. 8, and the $\dot{\boldsymbol{\varepsilon}}^{\boldsymbol{p}}$ is the strain increment tensor.

$$\boldsymbol{L} = \begin{bmatrix} \beta_{13} & -\beta_{12} + \beta_{13} & 0 & 0 & 0 \\ -\beta_{21} + \beta_{23} & \beta_{23} & 0 & 0 & 0 \\ -\beta_{31} & -\beta_{32} & 0 & 0 & 0 \\ 0 & 0 & \beta_{44} & 0 & 0 \\ 0 & 0 & 0 & \beta_{55} & 0 \\ 0 & 0 & 0 & 0 & \beta_{66} \end{bmatrix} \,. \quad (7)$$

The parameters β_{ij} are the transformation parameters that need to be optimized. The transformed equivalent plastic fracture strain can be determined by Eq. 8.

$$\dot{\varepsilon}_{eqv}^{T} = \sqrt{\frac{2}{3}\dot{\boldsymbol{\varepsilon}}_{eqv}^{T} : \dot{\boldsymbol{\varepsilon}}_{eqv}^{T}} \ . \tag{8}$$

The DF2016 fracture model accounts for both stress triaxiality and Lode parameter effects to describe the fracture mechanism [19]. The DF2016 criterion can be expressed as in Eq. 9 regarding the fully anisotropic fracture modeling approach.

$$\varepsilon_{eqv}^{T}(\eta, L) = \frac{c_3^a}{\left(\frac{2\tau_{max}}{\sigma_{eqv}}\right)^{c_1^a}\left(<\frac{\eta + c_4^a\frac{3-L}{3\sqrt{L^2+3}} + c^a}{\frac{1}{3} + c_4^a\frac{2}{3} + c^a}>\right)^{c_2^a}} \ . \tag{9}$$

In Eq. 7, η and L refer to stress triaxiality and Lode parameter, while the parameters $c_{1\text{-}4}$ and c denote the fracture model parameters.

Material Characterization

The parameters of the Yld2004-18p criterion were optimized based on the identification procedure explained in our earlier study [16]. For completeness of information, Table 2 lists the optimized parameters, and Fig.3 illustrates the analytical predictions of the yield criterion.

Table 2. The anisotropy parameters of Yld2004-18 criterion.

α_1'	α_2'	α_3'	α_4'	α_5'	α_6'	α_7'	α_8'	α_9'
0.396	0.43	0.824	0.747	-0.175	0.959	1	1	0.952
α_1''	α_2''	α_3''	α_4''	α_5''	α_6''	α_7''	α_8''	α_9''
0.655	1.507	0.683	0.837	1.465	0.87	1	1	0.983

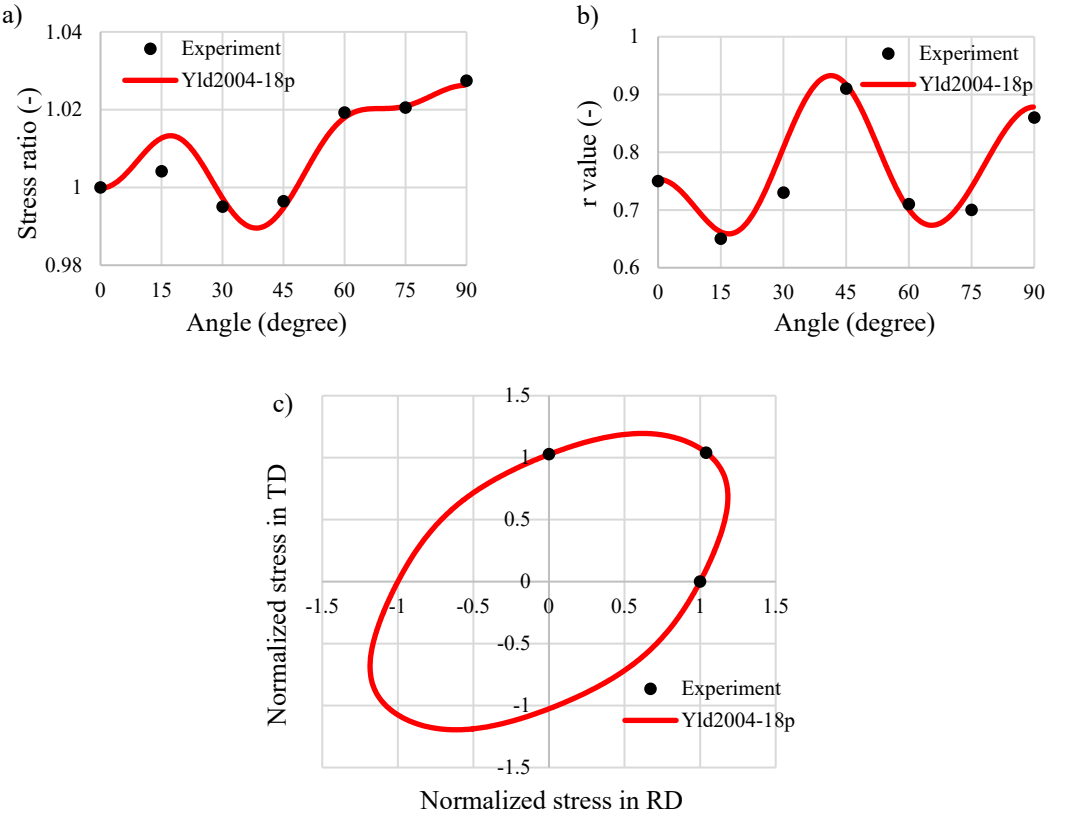

Fig. 3. Analytical predictions of Yld2004-18p a) Stress ratios, b) r values, c) yield locus.

The Yld2004-18p criterion accurately predicted the experimental data directionalities used in the identification procedure. The parameters and the flow curve fitted based on the mixed hardening

law can be found in ref. [10]. To calibrate the fracture model, the FE analyses of the fracture samples were conducted, and the acquired results were compared with the experimental outcomes. The element sizes were kept at 0.05 mm in all directions at the center of the geometrical discontinuities for each fracture sample [16]. Fig. 4 illustrates the comparative results of fracture samples' force-displacement responses for CH, NDBR10, and SH.

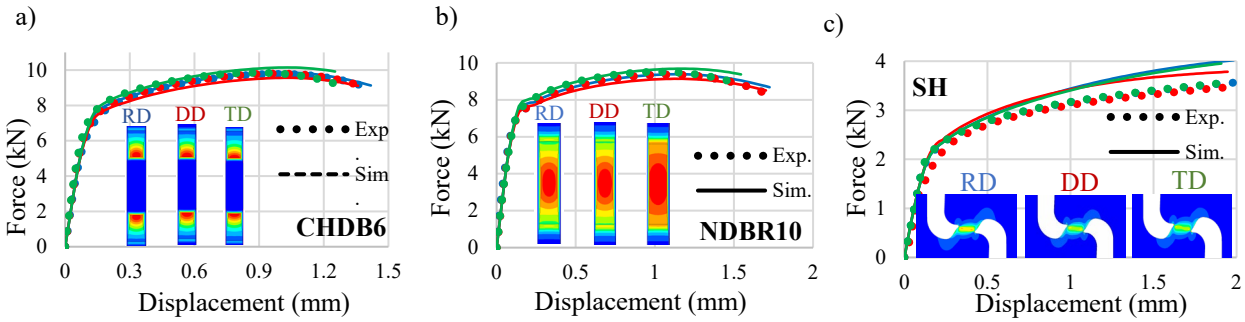

Fig. 4. Force-displacement predictions of the a) CHDB6, b) NDBR10, and c) SH samples.

The force-displacement predictions were consistent with experimental results. In CHDB6 and NDBR samples, the predicted results in RD and DD orientations provided good approximations; however, minor discrepancies were observed in TD orientation. In this regard, the implemented model could predict localization in RD and TD; however, it was less effective at predicting localization in TD. For NDBR samples, the maximum equivalent strain was seen at the center of the notched region, and at the middle of the through-thickness. For CHDB6 samples, it was found to be at the hole edge or a point so close to the hole edge (A minor shift was observed for RD and DD samples). As for SH samples, the maximum equivalent plastic strain at the shear zone was regarded. The plastic strain components, stress triaxiality, and Lode parameter variations were acquired from the FE simulations at fracture points of all samples. Since the Lode parameter and the triaxiality were not constant, their average values were determined. In the first stage, the transformations of the strain components were determined (In terms of transformation parameters); afterwards, the fracture model parameters and the transformation parameters were optimized simultaneously to calibrate the fully anisotropic fracture model. The optimized transformation parameters are listed in Table 3, while the 2D fracture locus alongside the variations of the stress triaxiality are given in Fig. 5.

Table 3. The transformation parameters for the fully anisotropic fracture model.

β_{12}	β_{13}	B_{21}	β_{23}	β_{31}	β_{32}	β_{44}	β_{55}	β_{66}
1.455	0.212	1.361	0.497	0.294	0.424	0.001	6.700	0.189

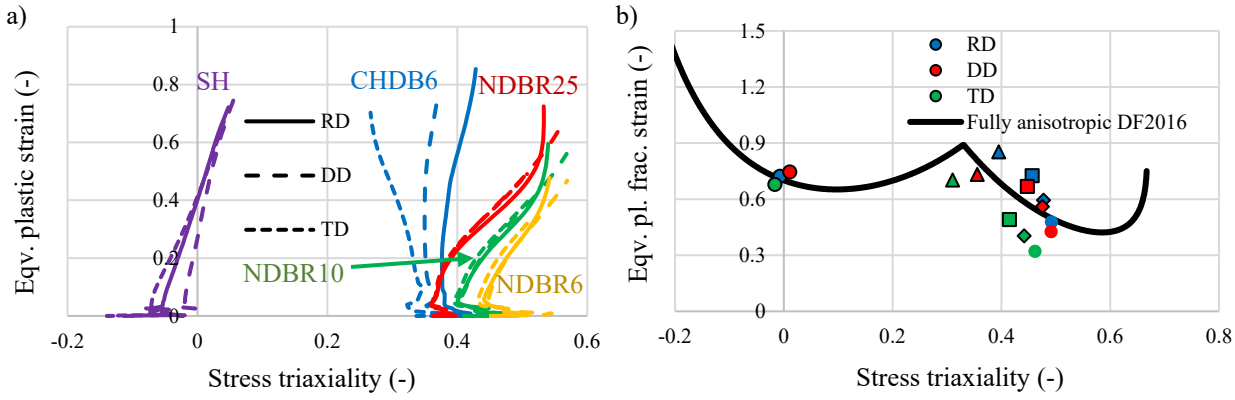

Fig. 5. a) Stress triaxiality variations, b) 2D fracture locus of fully anisotropic fracture model (The parameters of DF2016 are $C_1 = 4.12$, $C_2 = 0.63$, $C_3 = 0.89$, $C_4 = 0.241$, and $C = 0.33$).

The equivalent plastic fracture strains were depicted as dots with different shapes (Triangles, squares and rhombuses represent the CHDB6, NDBR25 NDBR10, respectively, while the circles at the left with black outline denote the SH and the circles at the right without outline refer to NDBR6 samples) in Fig. 5b. All these points correspond to the equivalent plastic fracture strain value for the mean stress triaxiality level of each fracture sample's cutting orientation. The 2D fracture locus generated by the fully anisotropic fracture model provided good approximations for each data point obtained from the sample and orientation. However, some difficulties were encountered while capturing the TD orientation data. These difficulties may stem from the fact that minor overestimations were observed in the force-displacement responses of the fracture samples of CHDB and NDBR (see Fig. 4). The implemented model could not successfully capture localization in the TD orientation. This situation may cause the fully anisotropic fracture locus to be offset downward during the optimization process. Since the force-displacement results in RD and DD were accurate and the localizations in these orientations were well characterized, higher strains may be obtained for these orientations compared to TD. Recently, in the paper by Li et al. [10], the researchers regarded the stress evolution during deformation and incorporated it into their FE simulations. Thus, they could capture the force-displacement responses in all orientations using the Hill48 criterion, and they reported higher strains and triaxiality levels in TD orientation compared to this study. Nevertheless, they also reported lower strain and triaxiality levels in TD than in RD and DD orientations in their research, consistent with the outcomes of this research. On the other hand, the results procured from the SH samples were also similar in all directions in this research. For each orientation, the equivalent plastic fracture strains and the stress triaxiality levels were close to each other. The differences in predicted performance for SH did not lead to a significant difference. Besides, although Li et al. [10] provided good approximations in SH samples considering the stress evolution, the SH results in this study were also consistent with the paper by Li et al in terms of strain and triaxiality levels. Afterward, the calibrated parameters were tested in fracture samples to predict the force drops in the simulations. Fig. 6 shows the results of force-displacement responses of fracture samples with the calibrated model.

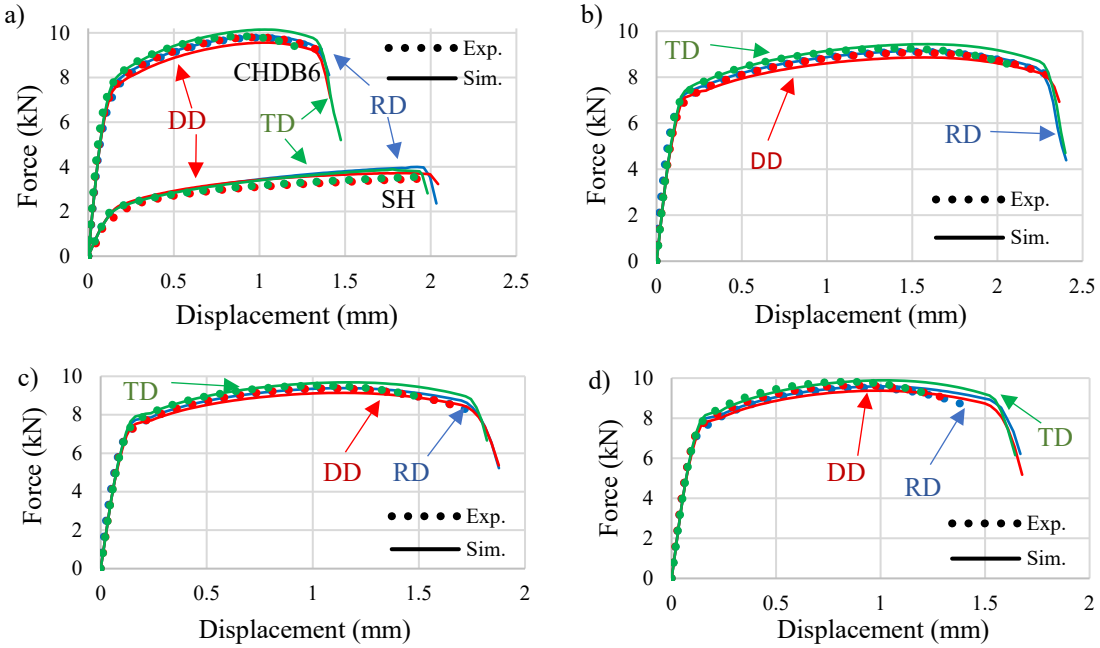

Fig. 6. Force-displacement predictions of fully anisotropic fracture model a) CHDB6 and SH, b) NDBR25, c) NDBR10, d) SH.

In NDBR6 predictions, the fully anisotropic fracture model overpredicted the experiments, which resulted from the difficulties in capturing the NDBR6 data alongside the TD data in the fracture locus. Nevertheless, the results were found to be consistent with the experiments for other samples.

Hole Expansion Test Simulations

The FE simulation of HET was carried out in Marc software coupled with a user-defined material subroutine. The blank was meshed in the Apex software, then transferred to the Marc software. The elements were increased near the hole edge, and the element sizes near the hole were kept 0.05 mm in all directions to ensure consistency with the element density in geometrical discontinuities of the fracture samples. Fig. 7 shows the FE model and the blank mesh.

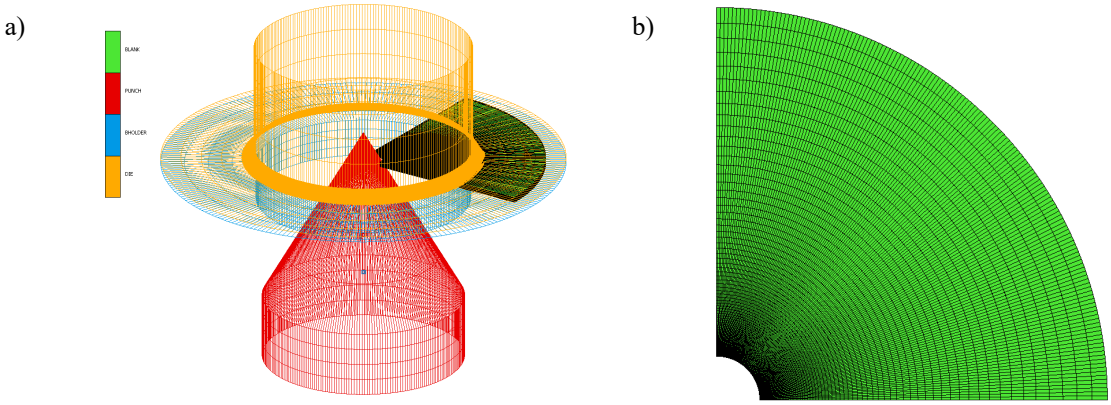

Fig. 7. a) FE model of HET, b) blank's mesh layout.

The friction coefficient was assumed to be 0.1 between all the contact interactions. The punch force-displacement curve, the first through-thickness crack, and the HER value were predicted by the FE model. Fig. 8 shows the metrics of local formability procured from the HET simulations.

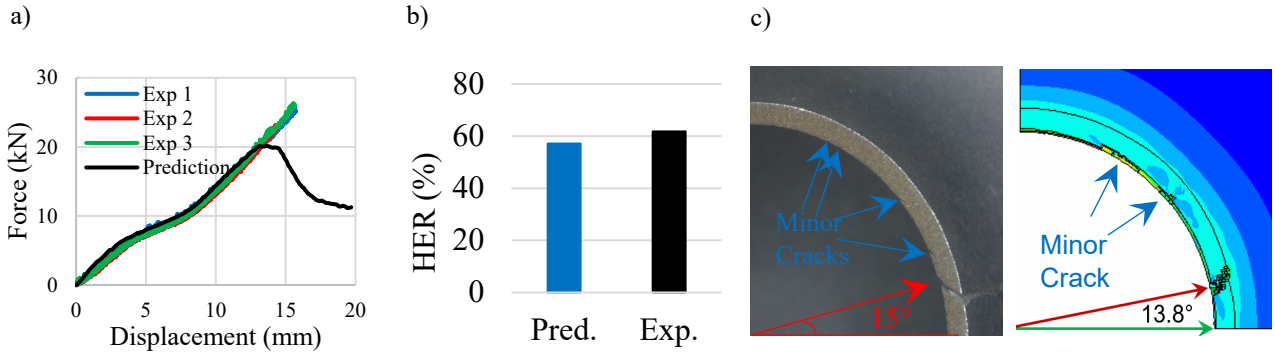

Fig. 8. a) Punch-force-displacement results, b) HER results, c) First TTC location.

The fully anisotropic model successfully predicted the first TTC location (Fig. 8b). Furthermore, minor cracks detected in the experiments were also observed near similar locations in the FE simulations. Underestimation of fracture force and HER values were still observed, which could be correlated with the performance of the fully anisotropic fracture model in tensile tests with different geometries. Further enhancement of the model formulation could improve the performance.

Conclusion

In this study, the local formability features of QP1000 steel were investigated through the HET of conical punch configuration. The fully anisotropic fracture model was implemented in order to characterize the material anisotropy and anisotropic ductility of the QP steel. Standard uniaxial tensile tests were conducted in seven orientations to calibrate the Yld2004-18p criterion, while five different fracture samples were tested in three orientations to define fully anisotropic fracture modeling. In the conical punch configuration of HET, the first TTC was observed at the hole edge. In the experiments conducted within the scope of this research, the first crack initiated at the hole edge's inner circle (punch side). In the following, the crack was progressed through the thickness in an inclined path. Initially, the inner circle is exposed to compression, then turns out to tension and high triaxiality regimes. During the progression of the crack, the stress state varies [16]. Therefore,

a wide range of fracture strain characterization extending from uniaxial compression to plane strain tension was found to be crucial. Moreover, the prediction of the fracture initiation zone alongside the inclination path of the crack is highly relevant to the anisotropic yield criterion. The results showed that the Yld2004-18p criterion well-defined the material anisotropy. Moreover, the fully anisotropic DF2016 fracture model showed plausible prediction performance. The implemented model predicted the first TTC location with high accuracy, indicating the advantages of introducing the anisotropy to both plasticity and fracture description, while further enhancement of the model is required for the force and hole expansion ratio at first through thickness crack. As a future remark, the stress evolution in all orientations can be regarded to adjust the anisotropic plasticity parameters better and describe the force-displacement response in the TD orientation. Accordingly, localization in the TD orientation may be accurately captured, thereby enhancing the fully anisotropic fracture model's performance in edge-cracking metrics.

Acknowledgement

Dr. Toros Arda Akşen would like to acknowledge the financial support provided by the Scientific and Technological Research Council of Türkiye (TÜBİTAK) under the 2219 – International Postdoctoral Research Fellowship Program [Grant Number: 1059B192400070].

References

[1] A.L.C. Ferrer, A.M.T. Thomé, Carbon emissions in transportation: a synthesis framework, Sustain 15 (2023) 8475.

[2] L Wang, J.G. Speer, (2013). Quenching and Partitioning Steel Heat Treatment. Metall. Microstruct. Anal. 2 (2013) 268-281.

[3] D.Q. Zou, S.H. Li, J. He, B. Gu, Y.F. Li, The deformation induced martensitic transformation and mechanical behavior of quenching and partitioning steels under complex loading process. Mater. Sci. Eng: A, 715 (2018) 243-256.

[4] K. Chung, N. Ma, T. Park, D. Kim, D. Yoo, C.A. Kim, A modified damage model for advanced high strength steel sheets, Int. J. Plast. 27 (2011) 1485-1511.

[5] Z. Li, Y. Chang, J. Rong, J. Min, J. Lian, J. Edge fracture of the first and third-generation high-strength steels: DP1000 and QP1000. *IOP Conf. Ser.: Mater. Sci. Eng.*, *1284* (2023) 012021.

[6] V.K. Barnwal, S.Y. Lee, S.Y. Yoon, J.H. Kim, F. Barlat, Fracture characteristics of advanced high strength steels during hole expansion test, Int. J. Fract. 224 (2020) 217-233.

[7] M. Firat, T.A. Akşen, B. Şener, E. Esener A numerical prediction for hole-splitting damage of DP steels based on plastic work criterion using a polynomial stress potential, Exp. Tech. 48 (2024) 501–522.

[8] Z. Li, Y. Chang, W. Liu, J. Lian, Predicting edge fracture in dual-phase steels: Significance of anisotropy-induced localization, Int. J. Mech. Sci. 274 (2024) 109255.

[9] M. Madrid, C.J. Van Tyne, S. Sriram, E.J. Pavlina, J. Hu, K.D. Clarke, Hole expansion ratio in intercritically annealed QP 980/1180 steel grades as a function of testing condition. IOP Conf Ser: Mater Sci Eng 418 (2018) 012083.

[10] Z. Li, F. Shen, Y. Liu, C. Hartmann, R. Norz, S. Münstermann, W. Volk, J. Min, J. Lian Anisotropic fracture behavior of the 3rd generation advanced high-strength – Quenching and Partitioning steels: Experiments and simulation, J. Mater. Res. Technol. 30 (2024) 9395–9414.

[11] Z. Li, Influence of anisotropy on edge fracture of advanced high strength steels, Doctoral Thesis. Department of Mechanical Engineering. Aalto University (2025) Finland.

[12] A. Kozłowska, G. Kokot, K. Matu,s A. Grajcar, Monitoring the phase evolution and fracture behavior of advanced multiphase QP steel using EBSD technique and digital image correlation, Theor. Appl. Fract. Mech. 133 (2024) 104520.

[13] C. Pelligra, J. Samei, S.B. Amirkhiz, L.G. Hector, D.S. Wilkinson, Microstrain partitioning. Transformation induced plasticity. and the evolution of damage during deformation of an austenitic-martensitic 1.5 GPa quench and partition steel, Mater. Sci. Eng.: A 895 (2024) 146181.

[14] E. Dai, Z. Lv, P. Yuan, G. Liu, N. Guo, Z. Liu, B. Tang, Ductile fracture of anisotropic QP980 steel sheet by using the isotropic/anisotropic modified Mohr-Coulomb models, Eng. Fract. Mech. 290 (2023) 109522.

[15] H. Akhtar, T.S. Alhalaybeh, X. Fang, S.U.D. Asbah, S. Chao, Y. Lou, Fracture modeling of QP980 steel: Evaluating the Rice–Tracey and DF2016 criteria under diverse loading states, Mater. 18 (2025) 1303.

[16] T.A. Aksen, Z. Li and J. Lian, Anisotropic characterization and modeling of quenching and partitioning steel: predicting formability and hole expansion performance: submitted for publication (2026).

[17] Information on https://doi.org/10.5281/zenodo.14609769.

[18] F. Barlat, H. Aretz, J.W. Yoon, M.E. Karabin, J.C. Brem, R.E. Dick, Linear transfomation-based anisotropic yield functions, Int. J. Plast. 21 (2005) 1009–1039.

[19] Y. Lou, L. Chen, T. Clausmeyer, E. Tekkaya, A.E. Yoon, Modeling of ductile fracture from shear to balanced biaxial biaxial tension for sheet metals, Int. J. Solids Struct. 112 (2017) 169–184.